Journal of Materials Chemistry A

ROYAL SOCIETY OF CHEMISTRY

PAPER

View Article Online
View Journal

Cite this: DOI: 10.1039/d5ta10456d

Nafion *vs.* Fumion: impact of ionomers on the alkaline oxygen evolution reaction

Mairead R. Brownell,[a] Kenta Kawashima,[a] Ashutosh Rana,[b] Hugo Celio,[c] Chikaodili E. Chukwuneke,[a] James H. Nguyen,[b] Nathaniel R. Miller,[d] Jeffrey E. Dick *[b] and C. Buddie Mullins[acefg]

As demand for renewable energy sources grows, it is increasingly important to develop cost-effective, stable, and efficient alternatives to fossil fuels. Alkaline water electrolysis provides an especially promising solution to this challenge. Alkaline water electrolyzers, while promising, continue to pose a number of barriers to their widespread commercial implementation. Powder-based electrocatalysts, for example, rely partially on ionomers, or charged binder materials, for their stability and ionic conductivity. Notably, the charge of the ionomer should be considered in the context of the oxygen evolution reaction, whose reactant is negatively charged hydroxide. Despite this, a negatively charged, proton-conducting ionomer, Nafion, is used as a binding agent in most alkaline electrolyzers. This discrepancy motivates a systematic evaluation of anion-conducting ionomers as electrode binders in alkaline oxygen evolution electrocatalysis to improve hydroxide transport and enable more reliable catalyst screening. Here, we compare the activity and stability of an Ir/C electrocatalyst prepared with Nafion, Fumion, and a 1 : 1 Nafion : Fumion mixed binder to clarify the role of ionomer charge. While Fumion-containing electrodes exhibit high apparent current densities during cyclic voltammetry and chronopotentiometry, a substantial portion of this response arises from ionomer degradation rather than sustained catalytic activity. In contrast, mixed-ionomer electrodes achieve high current densities while maintaining stability comparable to Nafion-bound electrodes. These findings highlight the critical influence of anion-exchange ionomers on both measured activity and stability and underscore the need to reevaluate electrocatalysts previously benchmarked using Nafion-based electrodes.

Received 23rd December 2025
Accepted 23rd March 2026

DOI: 10.1039/d5ta10456d

rsc.li/materials-a

Introduction

In recent years, investing in the development of green energy alternatives has become increasingly important to curb the effects of global warming. Water electrolysis, or water splitting, provides a promising alternative to fossil fuels because it generates molecular hydrogen.[1,2] When processed in a fuel cell, hydrogen generates water, thus making it a green energy source.[3] Because of this, studying water electrolysis, and more specifically the electrocatalysis occurring at both the electrolyzer cathode, which performs the hydrogen evolution reaction (HER), and the anode, responsible for the oxygen evolution reaction (OER), has been of interest.[1,4]

Acidic water electrolyzers provide conditions that promote superior activity of the hydrogen evolution reaction (HER) due to the abundance of protons (H^+), while exhibiting moderate overall stability.[5,6] However, these systems rely on expensive noble metal catalysts like IrO_2 and RuO_2.[2,4,5,7] Additionally, given the comparatively slow reaction kinetics of the OER and the harsh conditions of acidic media, it is beneficial for industrialized electrolysis to take place in alkaline conditions. Inducing water splitting in alkaline conditions is beneficial for three main reasons: (1) it allows for the use of more inexpensive and abundant transition metal electrocatalysts, (2) it improves the kinetics of the OER because the reactant is hydroxide (rather than water), and (3) the lifetimes of alkaline electrolyzers are superior to those of their acidic counterparts.[5,8,9] This means that only one O–H bond is broken in each reactant as opposed to the two bonds broken under acidic conditions, where the intact water molecule is the reactant.

An electrode containing a powder electrocatalyst is typically made by mixing the electrocatalyst, ionomer, solvent, and sometimes a conductive carbon material.[10,11] This electrode

[a]Department of Chemistry, The University of Texas at Austin, Austin, Texas 78712, USA. E-mail: mullins@che.utexas.edu
[b]Department of Chemistry, Purdue University, West Lafayette, Indiana 47907, USA
[c]Texas Materials Institute, The University of Texas at Austin, Texas 78712, USA
[d]Jackson School of Geosciences, The University of Texas at Austin, Austin, Texas 78712, USA
[e]McKetta Department of Chemical Engineering, The University of Texas at Austin, Austin, Texas 78712, USA
[f]Allen J. Bard Center for Electrochemistry, The University of Texas at Austin, Austin, Texas 78712, USA
[g]H2@UT, The University of Texas at Austin, Austin, Texas 78712, USA

preparation strategy is widely used for screening prototype electrocatalytic materials across a range of applications and is currently employed extensively in laboratory-scale studies of the alkaline OER. Ionomers are polymers containing a charged functional group that helps to facilitate the transport of reactants to the surface of the electrode.[12] Nafion, a proton-conducting ionomer, is the most accessible, commercially available electrode binder used for electrolysis in both acidic and alkaline conditions.[12] Nafion's overall negative charge makes it an appealing binder for use in acidic conditions because the negative charge facilitates mass transport of protons to the cathode surface for the efficient catalysis of the HER.[13] Contrastingly, mass transport of the negatively charged hydroxide reactant in alkaline OER is not supported by Nafion due to charge repulsion.[13] However, if alkaline electrolyzers instead implemented anion-conducting ionomers, mass transport of hydroxide to the surface of the electrode could improve. Despite the promise of improved reaction kinetics, the development and scale-up of effective anion-conducting ionomers is lacking compared to that of proton-conducting ionomers.[14] Anion-conducting ionomers have an overall positive charge, which allows them to act as both an electrode binder and a source of ionic conductivity for hydroxide ions passivating the electrode surface.[10,15] Consequently, fundamental studies aimed at understanding the behavior of anion-conducting ionomers under electrolysis conditions are essential for advancing alkaline OER electrocatalytic materials, particularly in the context of lab-scale electrocatalytic evaluations. Moreover, a systematic assessment of the effects of replacing Nafion with anion-conducting ionomers is critical for future electrocatalyst screening and for the rigorous reevaluation of electrocatalysts that were previously benchmarked using Nafion-based electrodes. Several anion-conducting ionomers (*e.g.*, Fumion, Aemion, Aemion+, PiperION) are available for use in electrolyzers today.[16,17] However, none of these ionomers exhibit mechanical stability comparable to Nafion.[12] Additionally, most anion-conducting ionomers are not produced in quantities large enough to support industrialized water electrolysis. Despite this, it is still worthwhile to understand the behavior of anion-conducting ionomers in comparison to Nafion, as a deeper understanding of the impact of ionomers on powder-type electrocatalyst activity could prompt further development and implementation of stable, commercially available anion-conducting ionomers. This study compares the OER activity and stability of anodes incorporating either Nafion or Fumion (a representative anion-conducting ionomer), using Ir/C as a model electrocatalyst. Here, Ir/C was deliberately selected as a constant reference catalyst, enabling the isolation of ionomer effects while minimizing variability arising from the electrocatalyst itself. The repeating structural units of these ionomers are exhibited in Fig. 1. We also mixed the ionomers together in one electrode ink to evaluate whether integrating Nafion's mechanical robustness with Fumion's anion conductivity can enhance both activity and stability. Cyclic voltammetry (CV) and chronopotentiometry (CP) were used to evaluate the intrinsic activity and stability of each anode. X-ray photoelectron spectroscopy (XPS) was used to gain insights into surface bonding and structure, while scanning electron microscopy (SEM) and electron dispersive spectroscopy (EDS) were used to determine changes to surface morphology and composition during electrolysis. Electrocatalyst stability was further evaluated by analyzing the electrolyte using inductively coupled plasma mass spectrometry (ICP-MS). Additionally, electrochemical mass spectrometry (ECMS) was employed to monitor the faradaic efficiency of the OER *in situ* for each electrode.

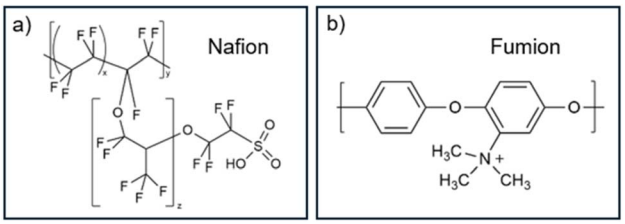

Fig. 1 Repeating structural subunits for (a) Nafion and (b) Fumion.

Materials and methods

Electrode preparation and cell setup

Bulk solutions containing 0.1% Nafion (Sigma-Aldrich, 5 wt%) or 0.1% Fumion (FAA-3-SOLUT-10, FuMA-Tech, 8–12 wt%) were made by diluting purchased stock solutions in isopropanol (Sigma-Aldrich, anhydrous, 99.5%) and sonicating for 30 minutes. Ir/C (fuel cell store, 20%) was used as the active catalyst and was incorporated into an electrode ink by sonicating 2 mg of the iridium catalyst in 1 mL of the ionomer solution for 30 minutes. A solution containing a 1 : 1 mixture of both the Nafion and Fumion solutions was made by first sonicating 2 mg of the iridium catalyst in 500 μL of Nafion bulk solution for 30 minutes. Then, 500 μL of the Fumion bulk solution was added, and the suspension was sonicated again for 15 minutes. Electrode inks were deposited onto the glassy carbon substrate of a rotating disk electrode (RDE) by dropcasting (0.122 mg cm^{-2}). The electrode was then allowed to dry at room temperature under vacuum for 30 minutes. A graphite counter electrode and Hg/HgO reference electrode (internal electrolyte: 1 M KOH), along with 125 mL of 1 M KOH, were used in the electrochemical cell. High surface area IrO_2 was used for making baseline measurements and was prepared using the same procedures (Grade S, Fuel Cell Store).

Electrochemical testing

The RDE was rotated at a rate of 1600 rot min^{-1} throughout cyclic voltammetry (CV), chronopotentiometry (CP), and electrochemical impedance spectroscopy (EIS) testing. Electrochemical performance and stability were assessed by conducting CV, CP, and double-layer capacitance measurements on a CHI600D Series Electrochemical Analyzer (CH Instruments). Each CV was performed following an ohmic drop compensation of 85%, and the electrode was cleaned with DI water between each CV test to remove residual bubbles within the electrode. Thoroughly rinsing the electrode ensured that degradation observed in the CV measurements could be attributed mainly to

changes at the electrode surface, although it is possible that some of this deactivation could be the result of microbubbles blocking the electrode surface. Double-layer capacitance values were compared between samples by taking the difference between the maximum and minimum current densities observed at 0.3 V (with ohmic drop compensation) and plotted *vs.* corresponding scan rates ranging from 10 to 200 mV s^{-1}. The electrochemically active surface area (ECSA) was then calculated by dividing the observed double layer capacitance by the specific capacitance of 0.040 mF cm^{-2}. Chronopotentiometry measurements were conducted at a current density of 10 mA cm^{-2} for 30 minutes or until the potential reached 1.5 V *vs.* Hg/HgO. Tafel slopes were determined by observing the slope between currents of 2.5 mA cm^{-2} and 6.3 mA cm^{-2}. EIS was performed on a stationary RDE using a potential of 0.65 V, and charge transfer resistances were calculated by determining the diameter of the curve in the Nyquist plot.

Electrochemical testing to quantify the molecular oxygen evolved, electrochemical mass spectrometry (ECMS), was conducted using a circular electrode, where the working electrode was prepared similarly to the cell setup described above. However, the cell setup differed greatly in that a flow cell was used to flow electrolyte through a thin channel between the working electrode and a semi-permeable membrane through which products could pass, thus allowing for a 100% collection efficiency measurement of electrocatalysis products. Additionally, due to instrumentation limitations, CP was collected at a current density of 0.5 mA cm^{-2}. Notably, Ag/AgCl [ET072-1 leakless miniature Ag/AgCl reference electrode (electrode potential: 204.63 mV at 21 °C; internal electrolyte: 3.4 M KCl), eDAQ][18] was used as a reference electrode while Pt was used as a counter electrode and were connected to a potentiostat (Biologic SP-300) controlled *via* EC-Lab software. During the experiment, helium (research purity 6N, A-OX Welding) was supplied through an internal mass flow controller. Zilien software (Spectro Inlets) was used for valve and mass spectrometer control and data collection. Data processing was carried out using the ixdat Python package for ECMS.

After collecting these data, faradaic efficiency was calculated by converting the moles of O_2 generated to moles of electrons used to generate molecular oxygen. The current *vs.* time plots collected from CV and CP measurements were used to calculate total charge transferred during the reaction by integrating under the curve. The charge was then converted to moles of electrons by dividing the total charge by Faraday's constant to obtain the total moles of electrons used in the measurement. The faradaic efficiency (FE) was then calculated using the following equation:

$$\mathrm{FE} = \text{mol } e^- \text{ to make } O_2 / \text{total mol } e^- \text{ transferred} \times 100\% \quad (1)$$

Characterization of the electrode

Morphology and general atomic makeup of the samples, both before and after CP testing, were determined using scanning electron microscopy (SEM, Apreo 2C) and electron dispersive X-ray spectroscopy (EDS, XFlash 7), and X-ray photoelectron spectroscopy (XPS, VersaProbe 4 and Axis Ultra DLD Kratos spectrometers). SEM and EDS were conducted on a RDE with a removable tip (generated in-house) and an acceleration voltage and current of 10 kV and 0.40 nA, respectively. In EDS, the electrode surface was scanned for carbon, iridium, oxygen, nitrogen, fluorine, and sulfur. Samples tested after electrolysis were prepared by conducting CP measurements on an ionomer film deposited on a rotating disk electrode. The film was then sonicated into a vial containing 1 mL of isopropanol. XPS was conducted using a carbon foil purchased from NeoGraf Solutions [Grafoil®, synthetic flexible graphite (thickness: 17 μm)]. The samples were prepared with the same loading as in electrochemical testing, but the ink was deposited on a 1 cm × 1.5 cm piece of graphite foil. Water electrolysis was conducted using a similar cell setup as with electrocatalytic cell measurements, but the electrolyte was mixed using a stir bar at 300 rpm. XPS was collected for films both before and after conducting chronopotentiometry for 30 minutes. Inductively coupled plasma mass spectrometry (quadrupole ICP-MS, 7500cc) was tested on the electrolyte after conducting chronopotentiometry measurements. The same cell assembly was used as in previous electrochemical testing, but the cell contained 50 mL of 1 M KOH. Samples were then homogenized by dissolving 35.7 μL in 10 mL of a 3% HNO_3 solution.

Results

Electrochemical testing

Initial electrochemical testing of Ir/C indicated that, after oxidation to IrO_2, the catalytic activity of the electrocatalyst film containing Fumion is slightly higher than that containing Nafion, as indicated by the overpotentials of 337 ± 5 and 349 ± 11 mV, respectively, all of which were observed at 10 mA cm^{-2} (Fig. 2a and S1–S3).[19–23] The sample with the mixed 1 : 1 Nafion : Fumion ionomer exhibited an overpotential of 322 ± 6 mV, which indicates noticeably higher activity than the sample containing solely Nafion. These results can be compared to a benchmark IrO_2 sample in Fig. S5a. This electrode also exhibits higher stability but lower activity than samples employing Ir/C as an electrocatalyst despite having a higher overall surface area (Fig. S5b–d). This is due to the presence of carbon, which increases electrode conductivity.[24] Additionally, the electrode containing Nafion has a notably longer activation period from Ir to the more OER active IrO_2, as indicated by the increased activity following the first three voltammograms. This could be attributed to the reduced transport through the electrode using only Nafion as a binder. Notably, the appearance of the film with mixed binder exhibited significantly less uniformity than the other two films, thus indicating some amount of phase separation (Fig. S6). It was also observed that, when cycled, the electrode with mixed binder surprisingly exhibited lower stability than either electrode employing just a single ionomer as a binder (Fig. S1–S4). Based on previous studies on the electrocatalyst and the conditions of the OER on electrode degradation, we hypothesize that this could be due to the effects of dissolution and redeposition.[25,26] Notably, the reduced

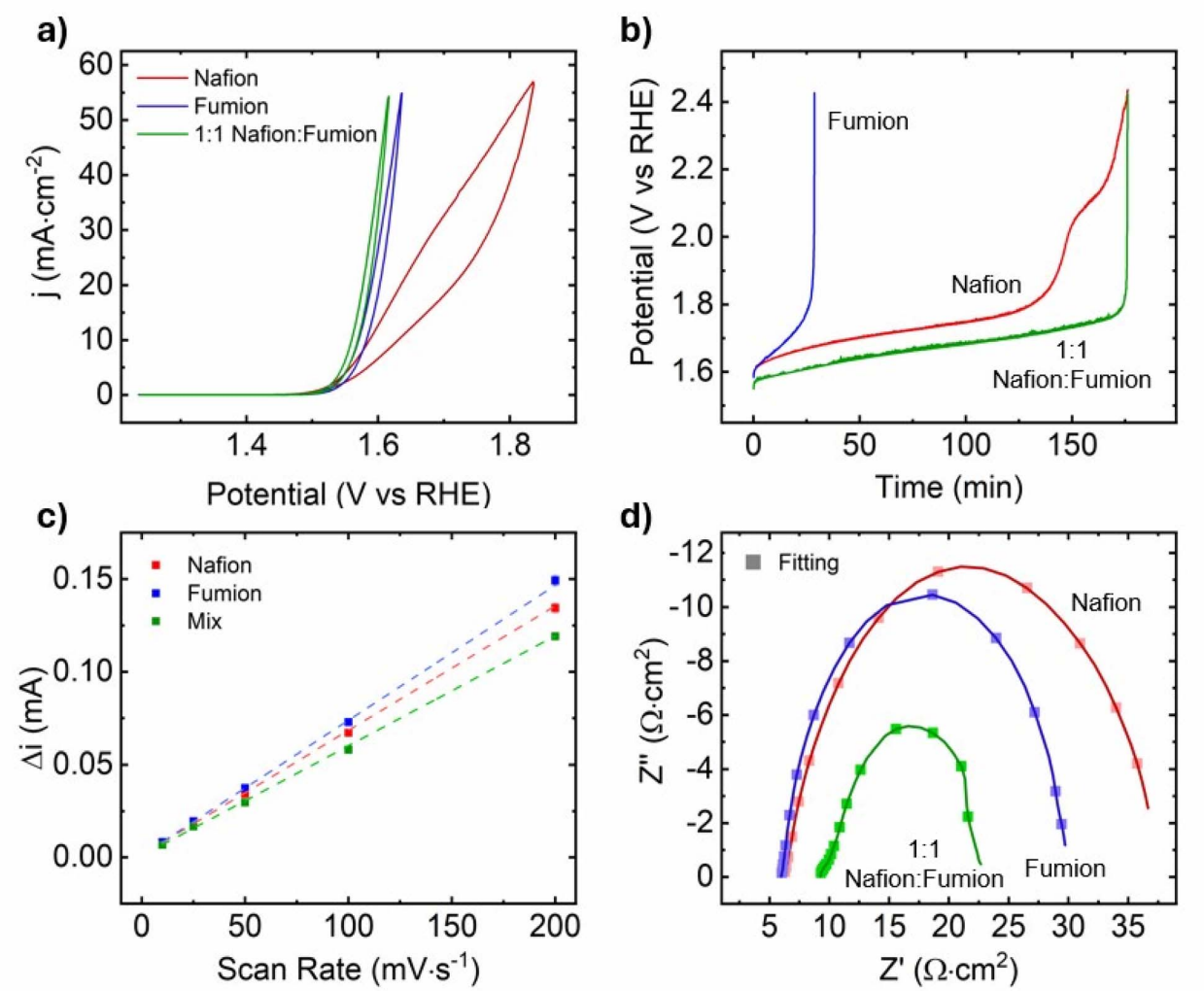

Fig. 2 (a) CV, (b) CP, (c) ECSA with linear fittings, and (d) EIS conducted on Ir/C electrocatalysts containing Nafion, Fumion, and 1 : 1 Nafion : Fumion ionomer in 1 M KOH electrolyte.

stability at cycling currents indicates that electrocatalyst dissolution is not followed by redeposition at potentials lower than that at which the OER begins. However, this hypothesis should be tested in a separate study to better understand the surface phenomena of this electrode. The Tafel slopes followed a similar trend to activity, as the samples containing Nafion, Fumion, and mixed binders exhibited Tafel slopes of 72.3, 47.7, and 39.0 mV dec^{-1}, respectively (Fig. S7). These results indicate that the intrinsic activity of the samples containing Fumion and mixed binders is more favorable than that of the sample containing Nafion. Importantly, at potentials exceeding the Tafel region, we observe increased differences in overpotential between the sample with a Nafion binder and the samples using both Fumion and mixed binders. In this region, mass transport of both the soluble product (H^+) and reactant (OH^-) should be considered. Incorporating both Nafion and Fumion into the electrode assists in supporting mass transport of both H^+ and OH^- through the pores of the electrode, ultimately improving overall OER kinetics.

While the electrode containing Fumion exhibited high activity, its stability was the lowest of the three samples when CP was conducted at a current density of 10 mA cm^{-2} (Fig. 2b). There are two factors likely contributing to the decreased stability observed in the Fumion-bound sample: (1) increased bubble retention, and (2) decreased ionomer stability. It has been reported previously that Fumion tends to develop a layer atop the electrocatalyst that can be challenging to penetrate.[27] Despite the dense layer of ionomer, both the positively charged functional group and the hydrophilic nature of Fumion allow for facile penetration of hydroxide to the electrode surface.[27] However, the hydrophobic nature of oxygen then prevents the product from evolving as efficiently from the surface.[28] In addition to bubble coverage being an issue, the susceptibility of Fumion to hydroxyl attack can result in dissolution of the electrocatalyst. The rapid degradation in electrocatalyst activity observed in Fig. 2b is well reported in previous studies, which suggest that higher current densities result in faster electrode deactivation.[26,29–31] The degradation pathways of similar anion-conducting pathways are reported in several previous studies,

and the instability observed in the CP curve is likely tied to the structure of Fumion.[32–35] Unlike Nafion, whose backbone consists mainly of strong, stable C–F bonds, Fumion is composed of a phenyl backbone connected by ether groups. The electron delocalization resulting from the phenyl groups provides stability during nucleophilic attack, allowing for oxidation of the backbone. Additionally, the electron-withdrawing properties of oxygen leave the bonded carbons electron-deficient, thus making them susceptible to attack by hydroxides. Notably, Fumion has a positively charged amine group that allows for nucleophilic attack at the surrounding carbons, thus contributing to Fumion's overall instability during electrocatalysis.

Electrochemically active surface area

While the initial data clearly indicate that the electrode using Fumion as a binder has superior performance to that of the sample containing Nafion, it is possible that the high current density could be attributed to two alternative factors: (1) differing electrode surface area and (2) oxidation of the ionomer. Because of this, it was necessary to conduct measurements to predict real surface area and faradaic efficiency. Cyclic voltammetry and electrochemical impedance spectroscopy (EIS) were used to determine the double-layer capacitance, which is often analogous to the real surface area of the electrode. While it is possible to calculate the real surface area of a planar transition metal electrode, for example, the real surface area cannot be calculated accurately with an electrode ink whose surface is covered with an ionomer layer.[36] Because of this, these measurements can only be used comparatively in this study. In the double layer capacitance measurements, the capacitive region is scanned at varying scan rates and plotted against the resulting current. Initial cycling measurements are plotted in Fig. S8. These results were then analyzed and plotted in Fig. 2c and indicate that the ECSAs of all three electrodes are roughly equivalent. When calculated empirically, the ECSA values were determined to be 16.8, 18.2, and 14.8 cm^2 for samples containing Nafion, Fumion, and mixed ionomer, respectively.[37] Current density observed in the CV curves in Fig. 2a were calculated using determined ECSA values and plotted in Fig. S9; these plots exhibit similar trends to those observed in Fig. 2a, thus supporting the finding that the Fumion- and mixed-ionomer containing catalysts exhibit better cycling activity to that of the Nafion-containing sample. While this finding is insightful, it is not exhaustive and cannot be solely relied upon. Because of this, it was necessary to conduct EIS to better characterize the reaction kinetics at the electrode surface. The impedance curve was modeled using a Randles circuit (Fig. S10). The resulting EIS is plotted in Fig. 2d, and the observed charge transfer resistances were extrapolated from the Nyquist plots. Charge transfer resistances for Nafion, Fumion, and mixed ionomer were 32.85, 24.66, and 14.14 Ω, respectively. These results indicate that the transfer of hydroxide to the electrode surface was improved by the presence of Fumion. Additionally, the further improved charge transfer resistance observed in the mixed ionomer sample could be due to improved charge transfer of generated protons through the membrane and back into the electrolyte following electrocatalysis.[38]

Faradaic efficiency

In addition to ECSA, faradaic efficiency was evaluated to determine the source of the current observed in CV and CP measurements. Electrochemical mass spectrometry (ECMS) was used to quantify oxygen produced during electrolysis. The charge required to produce O_2 was then compared to the total charge transferred in the reaction to determine the faradaic efficiency of the reaction. *In situ* faradaic efficiencies observed in CP measurements are plotted in Fig. S11–S13. Notably, faradaic efficiency resulting from CP and CV provides very different insights (Fig. 3 and S11–S26). The Fumion-containing sample, for example, exhibited much lower faradaic efficiency in CV (24.1%) compared to CP measurements (71.8%) (Fig. S15 and 3b). Given the surprisingly low observed currents and small

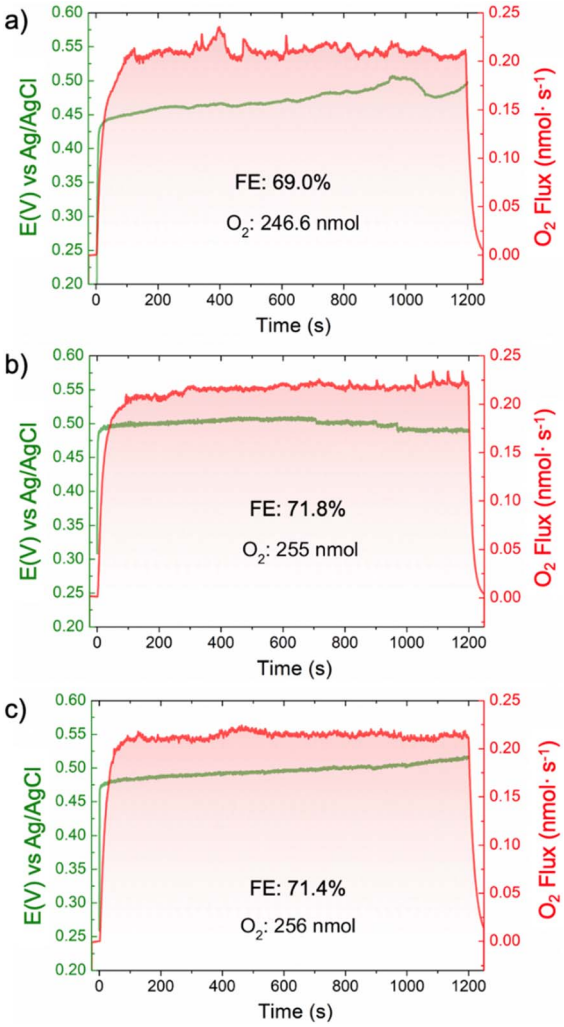

Fig. 3 ECMS measurement of oxygen evolved during chronopotentiometry measurements measured in 1 M KOH and collected at 0.5 mA cm^{-2} for samples containing (a) Nafion, (b) Fumion, and (c) mixed ionomer.

quantities of oxygen evolved using CV, we hypothesize that continuous cycling may result in bubbles being trapped in the first cycling measurements, thus reducing the ECSA and, in turn, the current and evolved oxygen quantities.[39] Observed behavior of the samples employing the Nafion and mixed binders was quite different from that of Fumion (Fig. 3a and c). Notably, the electrode with the mixed ionomer produced the highest volume of oxygen in both CV and CP measurements, exhibiting faradaic efficiencies of 72.1% during cycling and 71.4% during the CP testing (Fig. S16 and 3c). The sample with Nafion binder exhibited slightly lower faradaic efficiencies for both CV (67.0%) and CP (69.0%), an observation that may be partially attributed to the slower apparent activation of this sample (Fig. S17 and 3a). In addition to measuring evolved oxygen, carbon dioxide was also measured to determine if carbonaceous species were a source of parasitic reactions (Fig. S19–S26). However, the amount of CO_2 measured was negligible with respect to the total charge, thus indicating that most of the side reactions resulting in increased current likely produced soluble species. These results are particularly fascinating because they indicate that, not only does mixing Fumion into the Nafion-based electrode ink improve activity while maintaining stability, but it also affirms that the increased current observed can be attributed to the OER.

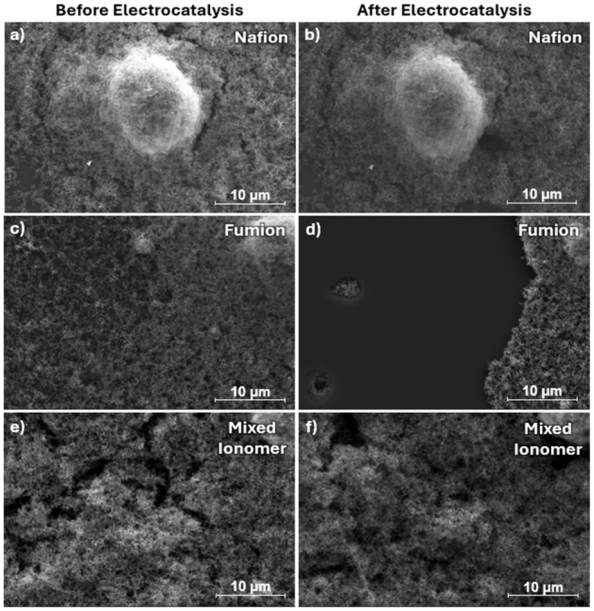

Fig. 4 SEM images showing changes to the electrode both before (left) and after (right) oxidation for samples containing (a and b) Nafion, (c and d) Fumion, and (e and f) 1 : 1 Nafion : Fumion. The images were captured at the same location before and after the OER test.

Electrode degradation

In addition to collecting electrochemical measurements, it was necessary to conduct a variety of characterization experiments to better understand electrode and ionomer behavior under oxidizing conditions. SEM and EDS were performed to observe physical and chemical changes in the electrode during CP measurements. The electrodes containing Nafion and mixed binder generally exhibited good mechanical stability and little physical detachment (Fig. 4a, b, e and f). Contrastingly, the electrode containing pure Fumion as a binder exhibited visible electrode detachment as observed in Fig. 4c and d. As expected, the oxygen signal observed in the EDS for all three samples increased upon oxidation (Fig. S27–S35). These results all support the observed CV and CP measurements.

While the SEM clearly indicated mechanical detachment of the electrode, ICP-MS of the electrolyte was conducted following electrode testing to determine the extent of mechanical detachment and the relationship between ionomer stability and electrocatalyst leaching. Unsurprisingly, the Nafion-containing sample exhibited the lowest concentration of iridium in the electrolyte (0.023 ppb) while the Fumion-containing sample exhibited the highest concentration of iridium in the electrolyte (0.056 ppb). The sample containing mixed ionomer surprisingly exhibited only slightly higher concentration of iridium than the Nafion-containing sample (0.029 ppb), which indicates that mixing the two ionomers helps to preserve the mechanical stability of the electrode.

While characterizing the entire electrode was important, it was also crucial to characterize the ionomer, specifically. This was done by conducting XPS measurements. The XPS spectra of the electrode containing Nafion indicate that the ionomer is relatively stable compared to that of Fumion when exposed to oxidizing conditions (Fig. 5a and b). Importantly, the additional C–C peak observed after electrocatalysis appears because of the variety of species containing C–C single bonds. As the ionomer layer diminishes slightly, the beam can probe the carbon black in the electrocatalyst. Unlike the ionomer, this species of carbon is grounded due to its high electronic conductivity, thus resulting in a slightly lower binding energy. The degradation of Nafion has been well reported previously.[40–43] Notably, the intensity of peaks in the spectra changes significantly (Fig. S36–S42). Fluorine spectra, for example, exhibit much lower intensity after oxidation, while sulfur peaks exhibit the opposite (Fig. S38 and S39). While it is difficult to draw conclusions from these results alone, spectral changes may be a result of a reduction in the thickness of the ionomer layer or re-orientation of the charged sulfur species at the surface of the electrode during electrolysis.[44] It is also important to note the increase in C–F_3 bond character following electrocatalysis because this indicates some amount of polymer oxidation, as the shifting to higher binding energy suggests the addition of some electron-withdrawing groups such as oxygen (Fig. 5b).[45] XPS spectra of Fumion, on the other hand, exhibit significant changes in intensity (Fig. 5c and d). Before electrocatalysis, there is a thin layer of ionomer on top of the electrocatalyst, as opposed to after electrocatalysis, where oxidation of Fumion causes polymer chain degradation, thus allowing for a slight increase in overall carbon signal resulting from Ir/C (Fig. 5c and d).[46,47] We hypothesize that this chain degradation occurs as a result of hydroxides attacking the electron-deficient carbon species bonded to the bridging oxygen atoms. The N 1s spectra perhaps exhibit most telling changes.[32] It has been well

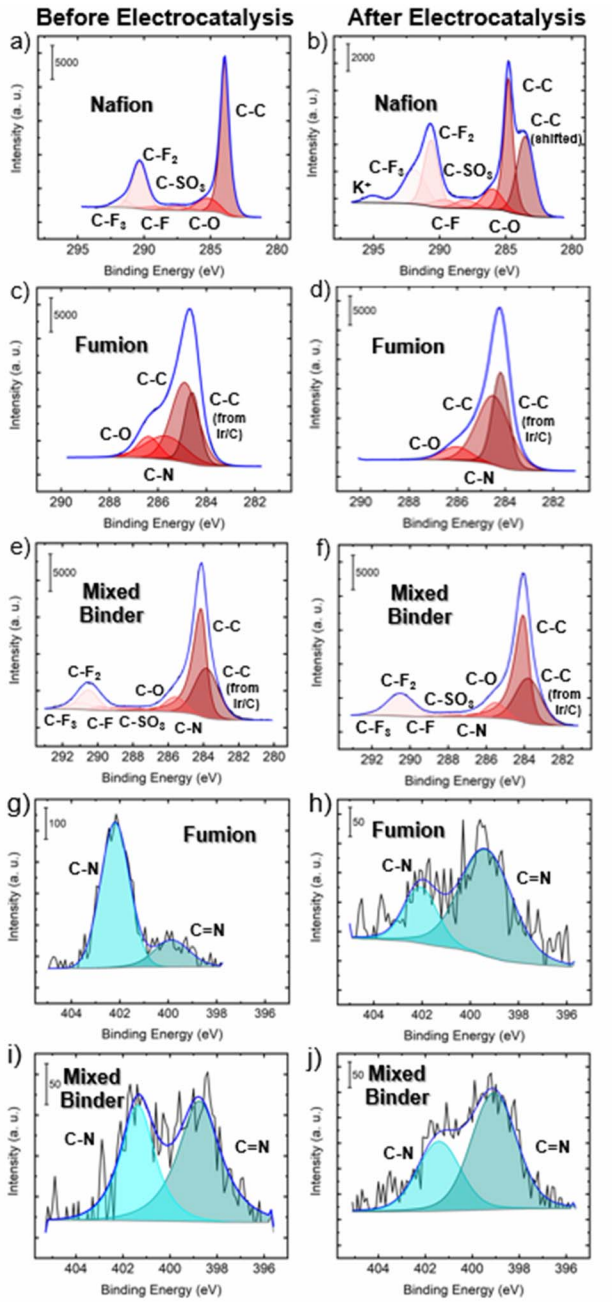

Fig. 5 (a–f) C 1s XPS spectra of dropcasted Ir/C electrodes with (a and b) Nafion, (c and d) Fumion, and (e and f) mixed ionomer both before (a, c and e) and after (b, d and f) electrocatalysis. (g–j) N 1s XPS spectra of dropcasted Ir/C electrodes with (g and h) Fumion, (i and j) mixed ionomer both before (g and i) and after (h and j) electrocatalysis.

documented in the literature that, in alkaline conditions, hydroxides tend to attack the carbon bonded to the positively charged functional group of the anion-conducting ionomers.[48–51] Much like electron-deficient carbon groups, the nitrogen-containing group ($[N(CH_3)_3]^+$) is susceptible to attack, thus making nucleophilic attack at the carbon within the ring competitive with attack at the nitrogen-bonded methyl groups. The electron delocalization at the ring allows for easier attack, thus making this process more thermodynamically and kinetically favorable.[52] However, there are three methyl groups at which to attack, thus making this an alternative pathway for degradation. The two proposed reaction pathways are as follows (where Bn stands for benzene):

Favored pathway:

$$Bn - [N(CH_3)_3]^+ + OH^- \rightarrow Bn - OH + N(CH_3)_3 \quad (2)$$

Alternative pathway:

$$Bn - [N(CH_3)_3]^+ + OH^- \rightarrow Bn - N(CH_3)_2 + CH_3OH \quad (3)$$

In eqn (2), the hydroxyl group attacks the ring, which results in the complete removal and dissolution of $N(CH_3)_3$. When a hydroxyl attack occurs at the methyl groups (eqn (3)), the methyl groups donate their electrons to nitrogen, which is reduced, thus resulting in an extra lone pair that can then be donated into the ring to create a carbon–nitrogen double bond. This is observed in the N 1s XPS, in which the large peak can be attributed to the carbon–nitrogen single bond, while the small peak in Fig. 5g, for example, indicates some small amount of nitrogen reduction at the charged group. However, the sample tested after electrolysis indicates a significant decrease in single bond character as a result of both reduction and complete removal of the charged nitrogen group (Fig. 5g and h). This observation is much less noticeable in the N 1s spectrum of the sample containing mixed binder, which indicates that mixing the binders provides some sort of protection against Fumion degradation (Fig. 5i and j). C 1s and F 1s spectra also exhibit minimal changes upon electrolysis, which could mean that, when mixed, both binders exhibit some stabilization. It should also be noted that all three spectra exhibit a notable increase in the iridium–oxygen bond, an observation that is expected due to the oxidation of iridium when exposed to anodic potentials (Fig. S37). First, a reduction in the thickness of the ionomer layer is expected to result in a higher overall Ir 4f signal following electrocatalysis. It is also well known that IrO_2 can degrade to IrO_4^{2-} and dissolve into the electrolyte under alkaline conditions, thus making it impossible to use XPS to draw any conclusions regarding chemical degradation of IrO_2 during electrocatalysis.[25]

Conclusions

In this study, two different ionomers were used to study the impact of charged functional groups on OER activity and stability. Although the same Ir/C electrocatalyst was used in both cases, the sample containing Fumion, a positively charged anion-conducting ionomer, exhibited superior electrocatalytic performance compared to Nafion, a proton-conducting ionomer. Contrastingly, chronopotentiometry indicated that the electrode bound by Fumion was the least stable compared to that of electrodes employing mixed ionomer and Nafion. Electrodes fabricated from mixed ionomers exhibited both superior activity and stability in CP testing. These results were supported by the measurements of faradaic efficiency. Further characterization, including ICP-MS, SEM, and EDS, confirmed that all

three electrodes were oxidized, while the electrode using solely Fumion as a binder experienced significant mechanical detachment and chemical degradation. XPS importantly indicated that Fumion was quite susceptible to attack by hydroxyl, thus resulting in significant degradation during testing. Despite the instability of Fumion in oxidative conditions, these results indicate the importance of developing more stable anion-conducting ionomers with commercial availability. This will allow academic researchers to better probe electrodes at a small scale first before scaling them for more application-based purposes. Additionally, promising results observed when the ionomers were mixed indicate the need for further research on both the behavior of the ionomer in the electrocatalyst ink, along with further understanding of interfacial interactions of ionomers at the electrocatalyst surface. Notably, this study underscores the critical issue regarding the OER activity of many previously reported powder-type electrocatalysts using Nafion binders may have been significantly underestimated. Furthermore, the apparent instability of such catalysts is likely attributed to ionomer degradation rather than intrinsic catalyst deterioration. Future investigations on powder-type electrocatalysts should rigorously account for the impact of ionomer properties when evaluating both activity and durability. However, it is also worth noting that, when investigating intrinsic electrocatalyst activity and stability, it is currently best to study electrocatalysts that do not require a binder. Additionally, the development of ionomers whose structure provides an inert environment that allows for more accurate probing of electrocatalyst function is paramount in advancing lab-scale development of new electrode materials.

Author contributions

Mairead R. Brownell: conceptualization, investigation, formal analysis, writing – original draft, writing – review & editing; Kenta Kawashima: conceptualization, writing – review & editing; Ashutosh Rana: investigation; Hugo Celio: investigation; Chikaodili E. Chukwuneke: investigation, writing – reviewing and editing; James Hoang Nguyen: investigation; Jeffrey E. Dick: project administration, writing – reviewing and editing; C. Buddie Mullins: project administration, funding acquisition, writing – review & editing.

Conflicts of interest

There are no conflicts to declare.

Data availability

The data acquired for composing this journal article are all contained in the main manuscript and the supporting information (SI). Supplementary information is available. See DOI: https://doi.org/10.1039/d5ta10456d.

Acknowledgements

The authors gratefully acknowledge the support of the National Science Foundation *via* Grant CHE-2102307 (CBM).

References

1 A. Vedrtnam, K. Kalauni and R. Pahwa, *Int. J. Hydrogen Energy*, 2025, **140**, 694–727.
2 H. Tüysüz, *Acc. Chem. Res.*, 2024, **57**(4), DOI: 10.1021/acsaccounts.3c00709.
3 N. A. A. Qasem and G. A. Q. Abdulrahman, *Int. J. Energy Res.*, 2024, **2024**, 7271748.
4 A. J. Shih, M. C. O. Monteiro, F. Dattila, D. Pavesi, M. Philips, A. H. M. Da Silva, R. E. Vos, K. Ojha, S. Park, O. Van Der Heijden, G. Marcandalli, A. Goyal, M. Villalba, X. Chen, G. T. K. K. Gunasooriya, I. McCrum, R. Mom, N. López and M. T. M. Koper, *Nat. Rev. Methods Primers*, 2022, **2**, 84.
5 S. Anantharaj and S. Noda, *Small*, 2020, **16**, 1905779.
6 A. Soni, S. K. Maurya and M. Malviya, *J. Power Sources*, 2025, **636**, 236571.
7 M. El-Shafie, *Results Eng.*, 2023, **20**, 101426.
8 Y. Guo, G. Li, J. Zhou and Y. Liu, *IOP Conf. Ser.: Earth Environ. Sci.*, 2019, **371**, 042022.
9 F. Lu, M. Zhou, Y. Zhou and X. Zeng, *Small*, 2017, 1701931.
10 E. Cossar, F. Murphy, J. Walia, A. Weck and E. A. Baranova, *Appl. Energy Mater.*, 2022, **5**, 9228–10330.
11 S. Martens, L. Asen, G. Ercolano, F. Dionigi, C. Zalitis, A. Hawkins, A. Martinez Bonastre, L. Seidl, A. C. Knoll, J. Sharman, P. Strasser, D. Jones and O. Schneider, *J. Power Sources*, 2018, **392**, 274–284.
12 S. Adhikari, M. K. Pagels, J. Y. Jeon and C. Bae, *Polymer*, 2020, **211**, 123080.
13 G.-F. Li, D. Yang and P.-Y. A. Chuang, *ACS Catal.*, 2018, **8**, 11688–11698.
14 N. Chen and Y. M. Lee, *Prog. Polym. Sci.*, 2021, **113**, 101345.
15 G. H. A. Wijaya, K. S. Im and S. Y. Nam, *Desalin. Water Treat.*, 2024, **320**, 100605.
16 C. Santoro, A. Lavacchi, P. Mustarelli, V. Di Noto, L. Elbaz, D. R. Dekel and F. Jaouen, *ChemSusChem*, 2022, **15**, e202200027.
17 L. J. Salazar-Gastelum, B. Y. Garcia-Limon, S. W. Lin, J. C. Calva-Yañez, A. Zizumbo-Lopez, T. Romero-Castañón, M. I. Salazar-Gastelum and S. Pérez-Sicairos, *Membranes*, 2022, **12**, 959.
18 K. Das, J. N. Hausmann, M. Driess and P. W. Menezes, *ACS Energy Lett.*, 2025, **10**, 3269–3274.
19 M. K. Horton, P. Huck, R. X. Yang, J. M. Munro, S. Dwaraknath, A. M. Ganose, R. S. Kingsbury, M. Wen, J. X. Shen, T. S. Mathis, A. D. Kaplan, K. Berket, J. Riebesell, J. George, A. S. Rosen, E. W. C. Spotte-Smith, M. J. McDermott, O. A. Cohen, A. Dunn, M. C. Kuner, G.-M. Rignanese, G. Petretto, D. Waroquiers, S. M. Griffin, J. B. Neaton, D. C. Chrzan, M. Asta, G. Hautier, S. Cholia, G. Ceder, S. P. Ong, A. Jain and K. A. Persson, *Nat. Mater.*, 2025, **24**, 1522–1532.

20 A. M. Patel, J. K. Nørskov, K. A. Persson and J. H. Montoya, *Phys. Chem. Chem. Phys.*, 2019, **21**, 25323–25327.
21 A. K. Singh, L. Zhou, A. Shinde, S. K. Suram, J. H. Montoya, D. Winston, J. M. Gregoire and K. A. Persson, *Chem. Mater.*, 2017, **29**, 10159–10167.
22 K. A. Persson, B. Waldwick, P. Lazic and G. Ceder, *Phys. Rev. B: Condens. Matter Mater. Phys.*, 2012, **85**, 235438.
23 A. Jain, S. P. Ong, G. Hautier, W. Chen, W. D. Richards, S. Dacek, S. Cholia, D. Gunter, D. Skinner, G. Ceder and K. A. Persson, *APL Mater.*, 2013, **1**, 011002.
24 A. Kumar, E. J. Park, Y. S. Kim and J. S. Spendelow, *Macro. Chem. Phys.*, 2024, **225**, 2400092.
25 A. Lončar, D. Escalera-López, S. Cherevko and N. Hodnik, *Angew. Chem., Int. Ed.*, 2022, **61**, e202114437.
26 X. Liu, Y. Bao, L. Yuan, H. Zhao, W. Tian and J. Ji, *J. Mater. Chem. A*, 2025, **13**, 35024–35053.
27 M. Liu, H. Hu, Y. Kong, I. Z. Montiel, V. Kolivoška, A. V. Rudnev, Y. Hou, R. Erni, S. Vesztergom and P. Broekmann, *Appl. Catal., B*, 2023, **335**, 122885.
28 E. Fois, A. Gamba and C. Redaelli, *J. Chem. Phys.*, 1999, **110**, 1025–1035.
29 T. H. Nga Ngo (Sarah Ngo), J. D. Riches, J. Love and A. P. O'Mullane, *ChemElectroChem*, 2025, **12**, e202400611.
30 H. A. El-Sayed, A. Weiß, L. F. Olbrich, G. P. Putro and H. A. Gasteiger, *J. Electrochem. Soc.*, 2019, **166**, F458–F464.
31 N. Kakati, L. Anderson, G. Li, D. M. Sua-an, A. Karmakar, J. D. Ocon and P.-Y. A. Chuang, *ACS Appl. Mater. Interfaces*, 2023, **15**, 55559–55569.
32 R. A. Krivina, G. A. Lindquist, S. R. Beaudoin, T. N. Stovall, W. L. Thompson, L. P. Twight, D. Marsh, J. Grzyb, K. Fabrizio, J. E. Hutchison and S. W. Boettcher, *Adv. Mater.*, 2022, **34**, 2203033.
33 C. Santoro, A. Lavacchi, P. Mustarelli, V. Di Noto, L. Elbaz, D. R. Dekel and F. Jaouen, *ChemSusChem*, 2022, **15**, e202200027.
34 Z. Tang, B. Wu, K. Yan, J. Luo, M. U. Haq and L. Zeng, *Future Batteries*, 2025, **5**, 100024.
35 N. Du, C. Roy, R. Peach, M. Turnbull, S. Thiele and C. Bock, *Chem. Rev.*, 2022, **122**, 11830–11895.
36 K. Wu, Z. Wang, G. Zhang, L. Fan, M. Zhu, X. Xie, Q. Du, B. Zu and K. Jiao, *Energy Convers. Manage.*, 2022, **251**, 114982.
37 C. C. L. McCrory, S. Jung, J. C. Peters and T. F. Jaramillo, *J. Am. Chem. Soc.*, 2013, **135**, 16977–16987.
38 X. Pan, M. Yan, Q. Liu, X. Zhou, X. Liao, C. Sun, J. Zhu, C. McAleese, P. Couture, M. K. Sharpe, R. Smith, N. Peng, J. England, S. C. E. Tsang, Y. Zhao and L. Mai, *Nat. Commun.*, 2024, **15**, 3354.
39 S. Favero, I. E. L. Stephens and M. Titirci, *Adv. Mater.*, 2024, **36**, 2308238.
40 M. J. Dzara, K. Artyushkova, J. Foster, H. Eskandari, Y. Chen, S. A. Mauger, P. Atanassov, K. Karan and S. Pylypenko, *J. Phys. Chem. C*, 2024, **128**, 8467–8482.
41 C. Chen, G. Levitin, D. W. Hess and T. F. Fuller, *J. Power Sources*, 2007, **169**, 288–295.
42 J. Foster, X. Lyu, A. Serov, S. Mauger, E. Padgett and S. Pylypenko, *Electrochim. Acta*, 2025, **517**, 145705.
43 S. Ben Jadi, A. El Guerraf, E. A. Bazzaoui, R. Wang, J. I. Martins and M. Bazzaoui, *J. Solid State Electrochem.*, 2019, **23**, 2423–2433.
44 P. Frühwirt, A. Kregar, J. T. Törring, T. Katrašnik and G. Gescheidt, *Phys. Chem. Chem. Phys.*, 2020, **22**, 5647–5666.
45 P. C. Okonkwo, I. Ben Belgacem, W. Emori and P. C. Uzoma, *Int. J. Hydrogen Energy*, 2021, **46**, 27956–27973.
46 Y. Xiao, W. Zheng, J. Wang, B. Li, P. Ming and C. Zhang, *Appl. Energy*, 2025, **389**, 125759.
47 G. Liu, D. McLaughlin, S. Thiele and C. Van Pham, *Chem. Eng. J.*, 2023, **460**, 141757.
48 Q. Li, M. Hu, C. Ge, Y. Yang, L. Xiao, L. Zhuang and H. D. Abruña, *Chem. Sci.*, 2023, **14**, 10429–10434.
49 R. A. Krivina, G. A. Lindquist, M. C. Yang, A. K. Cook, C. H. Hendon, A. R. Motz, C. Capuano, K. E. Ayers, J. E. Hutchison and S. W. Boettcher, *ACS Appl. Mater. Interfaces*, 2022, **14**, 18261–18274.
50 S. Favero, I. E. L. Stephens and M. Titirci, *Adv. Mater.*, 2024, **36**, 2308238.
51 I. Malone, S. Ünsal, R. S. Young, M. P. Jones, F. Spanu, S. Marathe, R. Jervis, H. G. C. Hamilton, C. M. Zalitis, T. S. Miller and A. J. E. Rettie, *Adv. Energy Mater.*, 2025, e01339.
52 K.-C. Lin, *J. Chem. Educ.*, 1988, **65**, 857.